Kinetic relaxation of giant vesicles validates diffusional softening in a binary lipid mixture

Kayla Sapp,[1] Mina Aleksanyan,[2,3] Kaitlyn Kerr,[1] Rumiana Dimova,[2] and Alexander Sodt[1]
[1]*Eunice Kennedy Shriver National Institute of Child Health and Human Development, National Institutes of Health, Bethesda, 20892 Maryland, USA*
[2]*Max Planck Institute of Colloids and Interfaces, 14476 Potsdam, Germany*
[3]*Institute for Chemistry and Biochemistry, Freie Universität Berlin, 14195 Berlin, Germany*

(Received 12 October 2022; accepted 15 March 2023; published 11 May 2023)

The stiffness of biological membranes determines the work required by cellular machinery to form and dismantle vesicles and other lipidic shapes. Model membrane stiffness can be determined from the equilibrium distribution of giant unilamellar vesicle surface undulations observable by phase contrast microscopy. With two or more components, lateral fluctuations of composition will couple to surface undulations depending on the curvature sensitivity of the constituent lipids. The result is a broader distribution of undulations whose complete relaxation is partially determined by lipid diffusion. In this work, kinetic analysis of the undulations of giant unilamellar vesicles made of phosphatidylcholine-phosphatidylethanolamine mixtures validates the molecular mechanism by which the membrane is made 25% softer than a single-component one. The mechanism is relevant to biological membranes, which have diverse and curvature-sensitive lipids.

DOI: 10.1103/PhysRevE.107.054403

I. INTRODUCTION

The cellular membrane is a complex mixture of many lipids and proteins, which may be attached peripherally, reside in one leaflet, or cross both. Membrane shape is highly influenced by a complicated cytoskeletal network. To isolate the mechanical effect of individual lipid components in such a system is currently infeasible. Giant unilamellar vesicles (GUVs) are an excellent membrane model system to which complexity can be introduced gradually [1]. Rather than attempting to visualize the distributions and motions of individual membrane components spectroscopically, with GUVs the influence of those components on the projected bilayer shape can be directly observed.

GUV mechanics are typically described using the Helfrich-Canham [2,3] (HC) energy density, H:

$$H_{\mathrm{HC}} = \frac{\kappa}{2}(c_1 + c_2 - c_0)^2 + \bar{\kappa} c_1 c_2, \tag{1}$$

where κ is the membrane bending rigidity, $c_1 + c_2$ is the total curvature where H_{HC} is being evaluated, $c_1 c_2$ is the Gaussian curvature, and c_0 is the bilayer spontaneous curvature.

We refer to the range of the magnitude of undulations of the GUV as the dynamic ensemble and to the relaxation times of the undulations as GUV kinetics. GUV mechanics are typically analyzed in terms of the dynamic ensemble. The bending stiffness is typically inferred from the range of the dynamic ensemble; larger fluctuations indicate a softer bilayer susceptible to thermal agitation. The stiffness also impacts kinetics; with a stronger restoring force, stiffer bilayers relax more quickly. The undulation of a GUV is visible to both phase contrast and confocal microscopy [4].

Some membrane mechanical parameters can also be inferred from static structures under external stress. An estimate of the stiffness of the red blood cell [5] as well as simple model membranes [6] can be obtained from analysis of the shape of membranes under micropipette aspiration. Even the challenging modulus of Gaussian curvature can be deduced from the analysis of the shapes of GUVs composed from a ternary mixture that phase separate into microscopic ordered and disordered domains [7]. In this case, the external stress is the line tension between domains, to which the shape of the surrounding vesicle adapts. The spontaneous curvature of lipid constituents can also be inferred by pulling nanoscale tubes using optically trapped beads. The force required for inward or outward tubulation will depend on the spontaneous curvature of the whole bilayer [8–10].

Setting aside the extreme case of macroscopic phase separation, lipid mixtures of complex molecular composition raise the possibility of lipid-lipid interactions giving rise to inhomogeneity invisible to microscopy. When nanometer-scale heterogeneity is a strong determinant of mechanical properties, the variation of lipid concentrations will modify the fluctuation spectrum of GUVs nonlinearly. The characterization of the effect of complex lipid heterogeneity by GUV fluctuations is closely related to the main target of interest: a model of the mechanics of cellular membranes.

This work examines a simple mechanism of softening in complex membranes, what we term diffusional softening [11]. Diffusional softening results from the dynamic coupling between the lateral distribution of lipids and the membrane undulations; an illustration of the mechanism is shown in Fig. 1. It has been proposed as a method for determining lipid or protein diffusion constants [12–14]. The mechanism only applies for leaflets with a mixture of lipids with varied spontaneous curvature. It is independent of the asymmetry of composition between leaflets. The effect was originally described by Leibler in 1986 for general inclusions [15], likely applicable to inclusions such as alamethicin [16], fusion peptides [17], and other proteins [14], but the theory

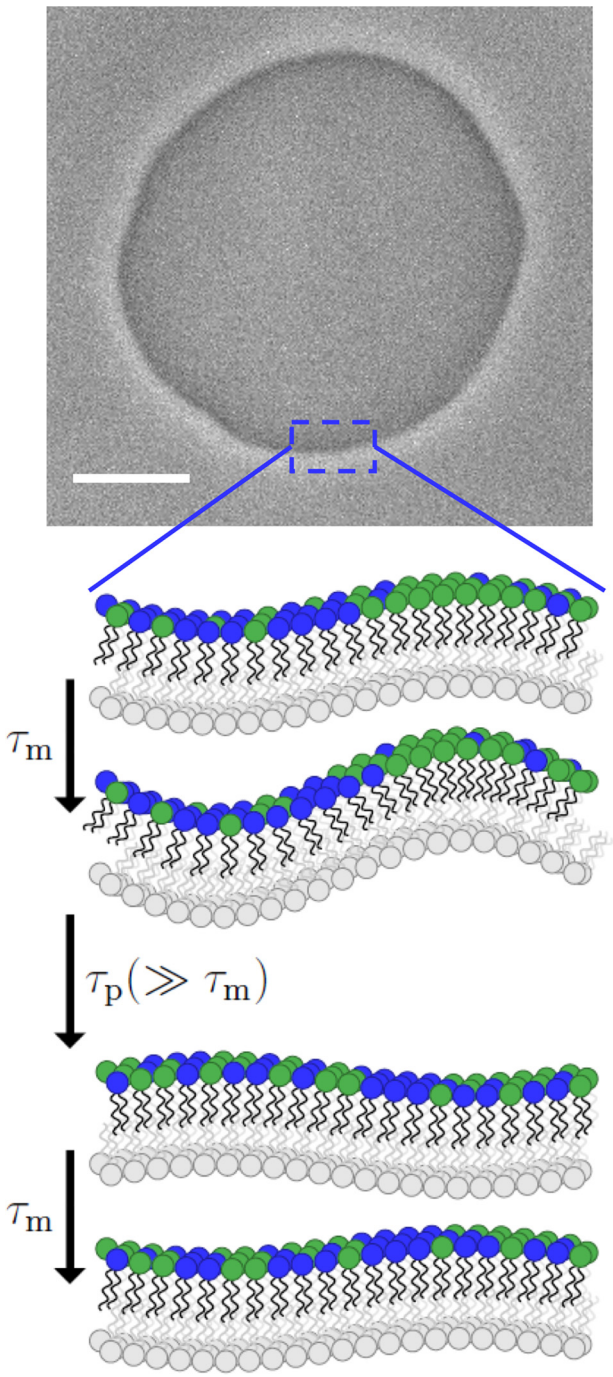

FIG. 1. A phase contrast screen shot of a quasispherical GUV composed of 40 mol% DOPE and 60 mol% POPC. The vesicle was prepared in 20 mM sucrose and diluted in 22 mM glucose. The scale bar is 10 m. Zooming in a patch on the vesicle can be considered planar. Consider the green (light gray) lipid to have more positive spontaneous curvature than the blue (darker gray). Stochastic colocalization of the green (light gray) lipid stimulates an undulation that adapts quickly (at the illustrated wavelength with relaxation time: τ_m). Over time, diffusion relaxes the lateral distribution (τ_p). The net effect is that the bilayer is softer both in appearance and practice. These fluctuations can be seen in S1 of the Supplemental Material [32].

applies equally well to lipids [12,18–20]. The width and relaxation time of nanotubes of lipid mixtures pulled from black lipid membranes strongly imply that lipid sorting leads to constriction of the tube, implying softness [21]. Nonlinear variation of κ has been observed in simple simulations of two component mixtures, in which the mixture of a stiff and soft lipid appears softer than even a pure bilayer of the soft lipid (see Fig. 3(a) of Ref. [22] and Fig. 8 of Ref. [23]). As shown below, the softening of κ is quadratic in the spontaneous curvature difference between lipids, and goes as $\chi(1-\chi)$, where χ is the mixed mole fraction for a binary mixture, consistent with the observations in Refs. [22,23].

Whereas the undulations of a single-component bilayer relax with time scale $\frac{r^3\eta}{\kappa}\frac{(2l+1)(2l^2+2l-1)}{(l-1)l^2(l+1)^2(l+2)}$, for diffusional softening the time scale is perturbed by the relaxation of the lateral compositional fluctuation, which goes as $\frac{r^2}{D_0}\frac{1}{l(l+1)}$. Here η is the solvent viscosity, l is the degree of the spherical harmonic (SH), r is the vesicle radius, and D_0 is the diffusion constant. This mechanism can thus be distinguished by the l dependence of the undulation relaxation time. The time scales also differ in their dependence on the vesicle radius.

The bending modulus for gel-phase systems approaches zero near the phase transition (see Fig. 13 of Ref. [24] and Fig. 6 of Ref. [25]). Thermal fluctuations of many mechanical properties are sufficient to explain this, including the area per lipid, which differs greatly between the gel and fluid phases. Differing curvature preference of gel and fluid phases would also contribute to bilayer softening. This is a clear indication of how dynamically fluctuating material properties lead to profound changes in softness. Moreover, the kinetics of the gel-fluid transition should influence the relaxation time of visible undulations. This work uses analysis of the kinetics of GUV relaxation, supported by simulation, to distinguish the intrinsic bending modulus from the diffusionally softened bending modulus.

The dynamic fluctuations of GUVs composed either completely of POPC or of 40% DOPE and 60% POPC are first presented. The reduced softness of the mixed system ($22k_BT$) compared to pure POPC ($28k_BT$) is shown to be consistent with diffusional softening on the basis of a kinetic fit to the autocorrelation function of the GUV undulation amplitude.

To validate the model, the kinetics of the relaxing GUV are compared to continuum simulations that incorporate the HC energy, as well as the experimentally validated relaxation times of the undulation and lateral-compositional fluctuations. Fitting the time dependence of autocorrelation functions is not straightforward. Choices of how to compare fits to the experimental data impact the accuracy and precision of the extracted model parameters. To account for this ambiguity in an evenhanded way, the expected error and optimal fitting strategy is derived from the simulations, rather than the experiments. Then, the fitting scheme is applied to the time autocorrelation function of GUV undulations, as measured by phase-contrast microscopy.

II. METHODS

The theory is first developed to describe the mechanism of diffusional softening, including the kinetics necessary for modeling. The experimental and simulation protocols for

characterizing GUV fluctuations are then provided, as well as how a framework was developed to most precisely fit the experiment as well as to anticipate stochastic error.

A. Theory

The HC energy density is modified by the presence of PE by subtracting the homogeneous (background) HC energy and adding in the contribution from the PE lipid:

$$H_{\mathrm{HC}}(\boldsymbol{r}) = \bar{H}_{\mathrm{HC}}(\boldsymbol{r}) + \Delta H_{\mathrm{PE}}(\boldsymbol{r}), \tag{2}$$

where

$$\bar{H}_{\mathrm{HC}}(\boldsymbol{r}) = \frac{\kappa}{2}(c_1(\boldsymbol{r}) + c_2(\boldsymbol{r}) - \bar{c}_0)^2 \tag{3}$$

and

$$\Delta H_{\mathrm{PE}}(\boldsymbol{r}) = \int_A d\boldsymbol{S}'\rho(\boldsymbol{r}')w(\boldsymbol{r}-\boldsymbol{r}')\frac{\kappa_{\mathrm{m}}}{2}[(c_1 + c_2 - c_{0,\mathrm{PE}})^2 - \times (c_1 + c_2 - \bar{c}_0)^2]. \tag{4}$$

Here $w(\boldsymbol{r})$ is the spatial extent of a single lipid [26] and $\rho(\boldsymbol{r}')$ is the number of PE lipids per unit area in the outer leaflet of the GUV (a trivial extension to both leaflets is made below). Note that the bending modulus is assumed to be homogeneous; the change in energy density only reflects changes in c_0. Assuming perfectly local spatial extent for a lipid,

$$w_{\mathrm{local}}(\boldsymbol{r}) = A_{\mathrm{p}}\delta(\boldsymbol{r}), \tag{5}$$

where A_{p} is the area of a PE lipid, yields

$$\Delta H_{\mathrm{PE}}(\boldsymbol{r}) = A_{\mathrm{p}}\rho(\boldsymbol{r})\frac{\kappa_{\mathrm{m}}}{2}[(c_1 + c_2 - c_{0,\mathrm{PE}})^2 - (c_1 + c_2 - \bar{c}_0)^2]. \tag{6}$$

$$= A_{\mathrm{p}}\rho(\boldsymbol{r})\frac{\kappa_{\mathrm{m}}}{2}(c_1 + c_2)\Delta c_{\mathrm{PE}} + \Delta H_{\mathrm{const.}}, \tag{7}$$

where $\Delta H_{\mathrm{const.}}$ is a constant term independent of vesicle curvature. The assumption of perfectly local extent is justified as long as the undulation wavelength considered is much greater than the mechanical extent of the lipid. According to the mechanical extent of simulated PE lipids [26], this is easily justified. larger lipidic patches requiring treatment at higher q could be described with finite spatial extent.

The average elastic curvature energy, without coupling to PE, is then

$$\bar{E}_{\mathrm{HC}} = \frac{\kappa}{2}\int_A d\boldsymbol{S}\bar{H}_{\mathrm{HC}}(\boldsymbol{r}). \tag{8}$$

For a vesicle, both the membrane shape $R(\theta,\phi)$ and lipid distribution $\rho(\theta,\phi)$ are expanded in SH:

$$R(\theta,\phi) = r\left(1 + \sum_{l=2}^{l_{\max}}\sum_{m=-l}^{m=l} u_{lm}Y_{lm}(\theta,\phi)\right) \tag{9}$$

$$\rho(\theta,\phi) = \rho_0 + \sum_{l=1}^{l_{\max}}\sum_{m=-l}^{m=l}\rho_{lm}Y_{lm}(\theta,\phi) \tag{10}$$

with coefficients u_{lm} (unitless) and ρ_{lm} (units per area). With the curvature written as the divergence of the normal, the compositionally averaged elastic energy $\bar{E}_{\mathrm{HC}}$ is evaluated from $\bar{H}_{\mathrm{HC}}(\boldsymbol{r})$ [Eq. (3)] as:

$$\bar{E}_{\mathrm{HC}} = \frac{\kappa}{2}\int dA(\nabla\cdot\boldsymbol{n})^2. \tag{11}$$

Taking a second-order approximation the curvature energy [Eq. (8)] is

$$\bar{E}_{\mathrm{HC}} = \frac{\kappa}{2}(l-1)l(l+1)(l+2)u_{lm}^2. \tag{12}$$

Given a bilayer with a mole fraction χ of one lipid (here DOPE) and $1-\chi$ background lipids (here, POPC), the energy of a density fluctuation is given by

$$E_\rho = \frac{A_{\mathrm{p}}r^2k_{\mathrm{B}}T}{4\chi(1-\chi)}\rho_{lm}^2. \tag{13}$$

This is a purely entropic factor.

The coupling of ρ_{lm} and u_{lm} by $\Delta H_{\mathrm{PE}}(\boldsymbol{r})$ is similarly evaluated in SH:

$$\Delta E_{\mathrm{PE}} = \kappa_{\mathrm{m}}\int dA\Delta c_{\mathrm{PE}}A_{\mathrm{p}}\rho_{lm}Y_{lm}\left(\nabla\cdot\boldsymbol{n} - \frac{2}{r}\right) \tag{14}$$

$$= \kappa_{\mathrm{m}}\Delta c_{\mathrm{PE}}A_{\mathrm{p}}r(l^2+l-2)u_{lm}\rho_{lm}. \tag{15}$$

Note that in our model, ΔE_{PE} for the inner leaflet of the bilayer requires only switching the sign of curvature; it is the negative of ΔE_{PE} for the outer leaflet. As the coupling depends linearly on ρ_{lm}, it is irrelevant whether lipids are modeled to be in the outer leaflet (with Δc_{PE}) or in the inner leaflet (with $-\Delta c_{\mathrm{PE}}$). We therefore state, without loss of generality, that they are distributed symmetrically throughout the bilayer as in the experiment. To further cast the model as the bilayer coupling, we reintroduce the bilayer κ, with $\kappa = 2\kappa_{\mathrm{m}}$:

$$\Delta E_{\mathrm{PE}} = \tfrac{1}{2}\kappa\Delta c_{\mathrm{PE}}A_{\mathrm{p}}r(l^2+l-2)u_{lm}\rho_{lm}. \tag{16}$$

Combining Eqs. (12), (13), and (16), the total energy is

$$E_{\mathrm{total}} = \bar{E}_{\mathrm{HC}} + E_\rho + \Delta E_{\mathrm{PE}}. \tag{17}$$

The expectation of u_{lm}^2 is determined by

$$\langle u_{lm}^2\rangle = Z^{-1}\int du_{lm}\int d\rho_{lm}u_{lm}^2e^{-E_{\mathrm{total}}/k_{\mathrm{B}}T}, \tag{18}$$

where

$$Z = \int du_{lm}\int d\rho_{lm}e^{-E_{\mathrm{total}}/k_{\mathrm{B}}T}. \tag{19}$$

For a single-component membrane ($\chi = 0$ or $\Delta c_{\mathrm{PE}} = 0$), integration leads to

$$\langle u_{lm}^2\rangle = \frac{k_{\mathrm{B}}T}{\kappa(l-1)l(l+1)(l+2)}, \tag{20}$$

from which the bending rigidity can be determined.

At higher q where diffusion is slower than the relaxation of undulations, the membrane autocorrelation function reflects the time scales of the two processes and how they are coupled through spontaneous curvature. We can derive a theoretical prediction of the autocorrelation function from the dynamics of the system.

The expectation of u_{lm}^2, ρ_{lm}^2, and $u_{lm}\rho_{lm}$ are

$$\langle u_{lm}^2\rangle = \frac{k_{\mathrm{B}}T}{\kappa(l-1)l(l+1)(l+1)}\left(1+\alpha+O\left[\Delta c_{\mathrm{PE}}^3\right]\right) \tag{21}$$

$$\langle \rho_{lm}^2\rangle = \frac{2\chi(1-\chi)}{A_{\mathrm{p}}r^2}\left(1+\alpha+O\left[\Delta c_{\mathrm{PE}}^3\right]\right) \tag{22}$$

$$\langle u_{lm}\rho_{lm}\rangle = \frac{\Delta c_{\mathrm{PE}}\chi(1-\chi)}{r(l+1)l}, \tag{23}$$

where the softening constant

$$\alpha = \frac{A_p \Delta c_{PE}^2 \kappa \chi(1-\chi)}{2k_B T} \frac{(l-1)(l+2)}{(l+1)l} \tag{24}$$

is defined for convenience, as it arises frequently.

A bilayer with a symmetric or asymmetric mixture of lipids (with unequal spontaneous curvatures) will experience apparent softening according to

$$\kappa_{\text{apparent}} = \kappa(1-\alpha). \tag{25}$$

Note that the fraction depending on l goes to one rapidly, giving the diffusional softening for a planar system [11,20]. This assumes that both leaflets contain the mixture $\chi = \rho A_p$.

Langevin equations model the kinetic relaxation of coupled membrane undulations and lipid redistribution. They are

$$\frac{\partial u_{lm}(t)}{\partial t} = -\Gamma_l \left(.\kappa(l-1)(l+2)(l(l+1))u_{lm} - \frac{1}{2} A_p \Delta c_{PE} \kappa (l^2+l-2) r \rho_{lm} \right) + \sqrt{2\Gamma_l k_B T}\xi(t) \tag{26}$$

$$\frac{\partial \rho_{lm}(t)}{\partial t} = -\frac{D}{k_B T} \left(\frac{A_p k_B T r^2 \rho_{lm}}{2\chi(1-\chi)} - \frac{1}{2} A_p \Delta c_{PE} \kappa (l^2+l-2) r u_{lm} \right) + \sqrt{2D}\xi(t), \tag{27}$$

where $\xi(t)$ describes a stochastic process:

$$\begin{aligned} \langle \xi(t) \rangle &= 0 \\ \langle \xi(t)\xi(t') \rangle &= \delta(t-t'). \end{aligned} \tag{28}$$

Note that when $u_{lm}(t)$ and $\rho_{lm}(t)$ are determined numerically below, $\xi(t)$ is simulated by drawing random numbers from a normal distribution with zero mean and variance Δt, where Δt is the time step. In Eq. (26), Γ_l describes the hydrodynamics associated with the membrane interacting with the solvent, and therefore depends on the solvent viscosity.

$$\Gamma_l = \frac{1}{\eta r^2} \frac{l(l+1)}{(2l+1)(2l^2+2l-1)}. \tag{29}$$

In Eq. (27), D:

$$D = \frac{D_0 \chi(1-\chi)}{A_p r^4} 2l(l+1) \tag{30}$$

is chosen to give the appropriate diffusion time scale. The symbolically simplified system of two overdamped harmonic oscillators, coupled together:

$$\begin{aligned} \frac{du_{lm}}{dt} &= -k_{hh} u_{lm} + k_{hp} \rho_{lm} \\ \frac{d\rho_{lm}}{dt} &= -k_{pp} \rho_{lm} + k_{ph} u_{lm}. \end{aligned} \tag{31}$$

Here k_{hh} and k_{hp} is proportional to η, while k_{ph} and k_{pp} are proportional to D. The sign of k_{hp} is positive indicating that amplitude in ρ_{lm} amplifies u_{lm}; this choice implies that curvature is measured in the sense of the upper leaflet; positive ρ_{lm} and positive c_0 imply that u_{lm} increases. This relationship is reversed in the lower leaflet (positive ρ_{lm} implies the lipid density is decreased in the lower leaflet).

Were curvature and diffusion independent, the two processes would have relaxation time scales:

$$\begin{aligned} \tau_m &= \frac{r^3 \eta}{\kappa} \frac{l^2(l+1)^2(l-1(l+2)}{2l+1)(2l^2+2l-1)} \\ \tau_p &= \frac{r^2}{D_0} \frac{1}{l(l+1)}. \end{aligned} \tag{32}$$

When diffusion is slower than shape fluctuations $k_{pp} \ll k_{hh}$ and the impact of coupling to the density depends on $k_{hp} \times k_{pp}$ as the density slowly impacts u_{lm}. The time autocorrelation function is

$$\langle u_{lm}(t) u_{lm}(0) \rangle = A_+ e^{(-k_+ t)} + A_- e^{(-k_- t)} \tag{33}$$

with decay constants

$$k_\pm = \tfrac{1}{2}\left(k_{hh} + k_{pp} \pm \sqrt{k_{hh}^2 - 2k_{hh}k_{pp} + k_{pp}^2 + 4k_{hp}k_{ph}}\right) \tag{34}$$

and time scales

$$\tau_{\pm,l} = k_\pm^{-1}. \tag{35}$$

For the purpose of interpreting the different time scales, consider τ_+ as the fast membrane relaxation time scale and τ_- as the slower diffusion time scale. $A_\pm$ are the amplitudes of each exponential.

With $k_{pp} \ll k_{hh}$ and k_{ph} small, to first order in the diffusion constant these rates are

$$\begin{aligned} k_+ &= k_{hh} - \frac{k_{hp}k_{ph}}{k_{hh}} = \frac{\kappa}{r^3\eta} \frac{(l-1)l^2(l+1)^2(l+2)}{(2l+1)(2l^2+2l-1)r^3} - \alpha \frac{D_0 l(l+1)}{r^2} + O\left[D_0^2\right] \\ k_- &= k_{pp} - \frac{k_{hp}k_{ph}}{k_{hh}} = \frac{D_0 l(l+1)}{r^2}(1-\alpha) + O\left[D_0^2\right]. \end{aligned} \tag{36}$$

The rates are both decreased by the coupling. The amplitudes associated with each exponential decay are

$$\begin{aligned} A_+ &= (1-\alpha) \\ A_- &= \alpha, \end{aligned} \tag{37}$$

where the autocorrelation function is normalized to be 1 at $t = 0$.

B. GUV microscopy

GUVs were prepared by the electroformation method as it is described previously [27,28]. Briefly, pure 1-palmitoyl-2-oleoyl-sn-glycero-3-phosphatidylcholine (POPC) (Avanti Polar Lipids, Germany) or a mixture of POPC and 40 mol% 1,2-dioleoyl-sn-glycero-3-phosphoethanolamine (DOPE) (Avanti Polar Lipids, Germany) were dissolved in chloroform to a final concentration of 4 mM. Then, 10 μL of the lipid solution was spread as a thin film on a pair of indium-tin oxide (ITO)-coated glass plates (PGO-GmbH, Iserlohn, Germany), which are electrically conductive. Afterwards, they were dried under a stream of nitrogen and placed in a desiccator for 2 h to evaporate the organic solvent. A Teflon spacer with 2 mm thickness was sandwiched between the two ITO glasses (conducting sides facing each other) to form a chamber. The chamber was filled with 20 mM sucrose solution and connected to a function generator (Agilent, Waldbronn, Germany). To initiate the

TABLE I. Simulation parameters.

Spontaneous Curvature, Δc_{PE} (nm^{-1})	0.0	0.140	0.280	0.340
Surface Coverage, χ	N/A	0.4		
Bending Rigidity, κ (units of $k_B T$)		33.78		
Diffusion Constant, D (μm^2/s)	N/A	8.0		
Viscosity, η (Pa s)		8.9×10^{-4}		
Area per Lipid, A_p (nm^2)		0.634		

electroswelling process, a sinusoidal alternating current (ac) electric field at 10 Hz frequency with a 1.6 V (peak-to-peak) amplitude was applied for 1 h. The obtained vesicles were harvested from the chamber and used freshly within 24 h after preparation. For fluctuation spectroscopy, the vesicle suspension was fourfold diluted in 22 mM glucose. The osmolarity of the sugar solutions was adjusted with osmometer (Osmomat 3000, Gonotec, Germany). The vesicles were additionally deflated before imaging by leaving the observation chamber open for 5 min to let water evaporate. Membrane fluctuations were observed under a phase contrast mode of an inverted microscope, Axio Observer D1 (Zeiss, Germany), equipped with a Ph2 40 x (0.6 NA) objective. High-speed video recordings were performed with a Pco. Edge camera (PCO AG, Kelheim, Germany). The image acquisition rate was set to 100 frames per second (fps) at exposure time of 200 ms. To prevent correlated images, statistics were averaged for every fourth frame. Only defect-free quasispherical vesicles, 8–21 μm in radius and with low tension values 10^{-7}–10^{-9} N m^{-1} were analyzed. A set of 21000 images (3×7000 frames with 3 min gap between each recording sequence) were acquired for each vesicle. All experiments were performed at 25 °C. The vesicle contour was detected through the laboratory-owned software [29]. This included software for the construction of spatial and temporal correlation functions to characterize the shape fluctuations of the membrane. Vesicle contours were detected through the Viterbi algorithm. The amplitudes were fit with the Levenberg-Marquardt algorithm for statistical analysis and characterization of κ_{apparent}. A χ^2 test was applied to determine the range of modes included, with values in the range of 0.8–1.2.

C. Simulation

Solving Eqs. (26) and (27) numerically for small discrete time increments leads to a time series for the membrane and distribution modes. The amplitudes of undulations are projected into the equatorial plane

$$v_n = \sum_{l=n}^{l_{\max}} u_{ln} P_{ln}(\cos \pi/2) N_{ln}, \tag{38}$$

where, P_{ln} are the associated Legendre polynomials and $N_{ln} = \sqrt{(2l+1)(l-n)!/4\pi(l+n)!}$ is a normalization factor. Four sets of simulations using parameters to reflect the experiments performed were done, values are in Table I. The time step is determined by the fastest membrane undulation mode ($\Delta t \ll \tau_{m,\min}$).

The undulation time autocorrelation function $[\langle v_n(t) v_n(0)\rangle]$ is calculated from the time series of membrane

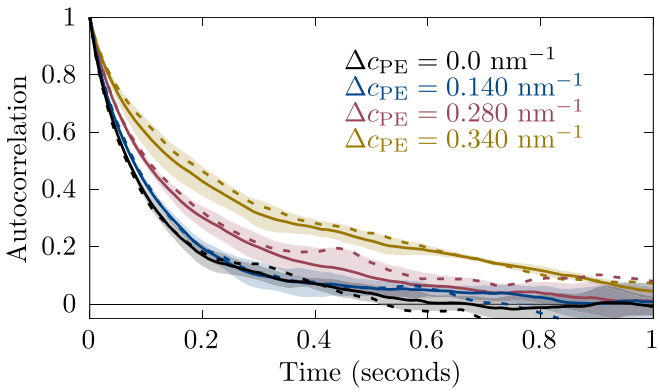

FIG. 2. An example of autocorrelation functions from simulation (for $q = 0.515$ μm^{-1}). Solid lines are averaged over three runs and dashed lines are for a single run. The shaded region is the standard deviation of the average. Here $\kappa = 33.8 k_B T$ and $D = 8\,\mu$m^2/s.

undulations. This is related to the autocorrelation function of the vesicle through the projection of the average amplitudes

$$\langle v_n(t) v_n(0)\rangle = \sum_{l=n}^{l_{\max}} \langle u_{ln}(t) u_{ln}(0)\rangle [P_{ln}(\cos \pi/2) N_{ln}]^2 \tag{39}$$

$$= \sum_{l=n}^{l_{\max}} \langle |u_{ln}|^2\rangle [P_{ln}(\cos \pi/2) N_{ln}]^2 e^{-t/\tau_l}. \tag{40}$$

This can be fit with the analytical expression derived above in order to extract the softening factor.

An example correlation function is shown in Fig. 2, where a single short time simulation spectrum (dashed lines) is compared to the average of three simulations (solid lines). Obviously, the single simulation spectrum contains a lot of noise. The experimental spectra are also overlaid with noise. For this reason, we average over three simulations to decrease the noise in the simulation spectrum. This allows for the determination of fitting parameters that can be used with experiment.

D. Fitting experimental and simulation autocorrelation functions

Autocorrelation functions are fit using a functional form that replicates the theoretical dynamics implied by Eqs. (36) and (37). These relations govern the dynamics of the complete SH, yet the functional form must be for the projection into the plane, just as the simulations replicate the observable of the GUV microscopy.

Autocorrelation functions for each vesicle projection are fit by a function

$$f_n(t) = w_{\text{fast}} \delta(t) + N_{\text{auto},n} \sum_{l=n}^{l_{\max}} |P_{ln}(\cos(\pi/2) N_{ln}|^2 \times \left(w_+ \exp\left(-\frac{t}{\tau_{+,l}}\right) + w_- \exp\left(-\frac{t}{\tau_{-,l}}\right)\right), \tag{41}$$

where $\delta(t)$ accounts for fast stochastic experimental noise, $\tau_{+,l}$ and $\tau_{-,l}$ are the membrane-dominated and

diffusion-dominated relaxation times, respectively [Eqs. (35) and (36)] while the w constants are weights:

$$w_+ = A_+(1 - w_{\text{fast}}) \tag{42}$$

$$w_- = A_-(1 - w_{\text{fast}}) \tag{43}$$

such that (with $A_+ + A_- = 1$) the weights sum to one. The constant

$$N_{\text{auto},n} = \left(\sum_{l=n}^{l_{\max}} |P_{ln}(\cos(\pi/2)N_{ln}|^2 \right)^{-1} \tag{44}$$

normalizes the autocorrelation function. The diffusion constant D, bending modulus κ, difference in spontaneous curvature Δc_{PE} are shared parameters for the set of autocorrelation functions. Additionally, a constant modeling the magnitude of unresolvable fast (below 0.01 seconds) noise w_{fast} is introduced for each correlation function.

Note that n denotes the integer mode of the projected spherical harmonic, which does not decay with a single time scale even absent particle coupling. Instead, it reflects the relaxation of spherical harmonics with $l \geqslant n$. However, the majority of the amplitude will be dominated by the lowest mode spherical harmonic with $l = n$. Therefore, we attach the wave number $q = \frac{n}{R}$ to describe autocorrelations of v_n, expecting the dynamics of modes with similar q but with varied n on vesicles of varied R to have similar kinetics. We use q to define the range of modes appropriate for fitting with the above theoretical kinetics, as well as to shift the weight bye w_q of autocorrelation functions in χ^2 to higher q. With their fast relaxation times, autocorrelation functions at higher q have compressed time domains and thus contribute weakly to χ^2.

Optimal parameters are found by minimizing

$$\chi^2 = \sum_i w_q \sum_{t=0}^{t<t_{\max,q}} [f_{n,i}(t) - v_{n,i}(t)]^2, \tag{45}$$

where the sum is over all autocorrelation functions for a vesicle set with q such that $q_{\min} < q < q_{\max}$. Here $t_{\max,q}$ depends on q. The time domain is chosen in terms of n multiples of the membrane relaxation time, $t_{\max,q} = n\tau_{\text{m}}$.

We use a sum of exponentials, one with τ_{m} and one with τ_{p}. The difference between these mechanisms is their q dependence (q^{-3} vs. q^{-2}). Practically, we fit the data with the bending modulus and diffusion constants as two adjustable parameters. In the two-parameter fit each mode has an additional parameter: the weight of autocorrelation that is assigned to the diffusion mechanism.

III. RESULTS AND DISCUSSION

The diffusional softening mechanism derived is tested on both simulation and GUV fluctuation data by fitting fluctuation autocorrelation functions to the model [Eq. (41)]. Fitting yields the apparent spontaneous curvature difference (Δc_{PE}), intrinsic bending rigidity (κ), and lipid diffusion constant (D), extracted purely from kinetics. Typically, κ_{apparent} [equal to $(1 - \alpha)\kappa$] would be determined from the average fluctuations ($\langle v_n^2 \rangle$). In addition to the kinetic analysis that determines κ and Δc_{PE} and thus implies κ_{apparent}, fluctuation analysis applied to determine κ_{apparent} is shown below.

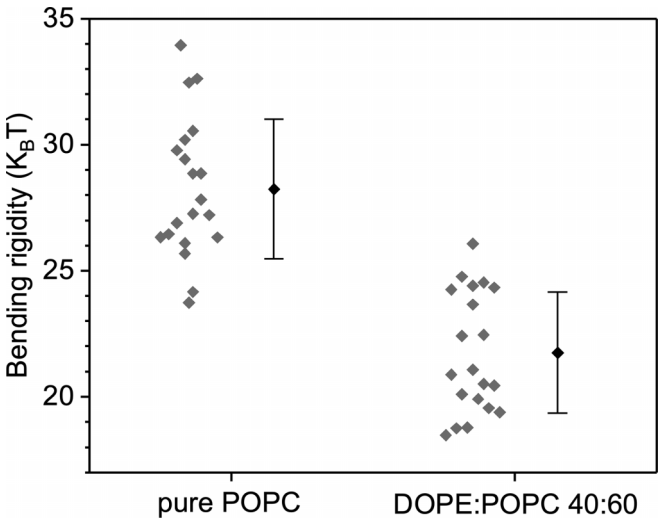

FIG. 3. Bending rigidity of membranes made of pure POPC (100 mol%) and DOPE:POPC 40:60 mol%. Gray diamonds indicate measurements on individual GUVs. Mean and standard deviation values are shown to the right.

A. Apparent bending rigidity from GUV fluctuations

The classic GUV fluctuation experiment extracts the bending modulus from equilibrium fluctuations ($\langle v_n^2 \rangle$):

$$\frac{\kappa_{\text{apparent}}}{k_{\text{B}}T} = \frac{\sum_{l=n}^{l_{\max}} \frac{(P_{ln}(\cos\pi/2)N_{ln})^2}{(l+2)(l-1)(l(l+1)+\tilde{\sigma})}}{\langle v_n^2 \rangle}. \tag{46}$$

The bending modulus and tension are fit as in Ref. [29]. Following determination of each individual vesicle κ_{apparent} by fluctuation analysis, two sets of similar vesicles were determined, one for each composition. The range in κ_{apparent} for inclusion into the sets was determined by sorting the vesicles according to κ_{apparent} and selecting a range with minimal variation in κ_{apparent}. A set of GUVs with similar apparent bending modulus were selected for analysis, one for PE-PC (eight vesicles with κ_{apparent} from 19.59–21.28 $k_{\text{B}}T$ with mean 20.27 ± 1.18 $k_{\text{B}}T$) and one for POPC (nine vesicles with κ_{apparent} from 26.01–28.21 $k_{\text{B}}T$ with mean 26.69 ± 1.86 $k_{\text{B}}T$). The rationale is that variations in bending modulus, for whatever reason, would imply a variation in relaxation time scale, although the time scales would still be well separated. Averaging over all the GUVs, the κ_{apparent} for PE-PC was 21.74 ± 2.52 $k_{\text{B}}T$ and for POPC was 28.24 ± 3.19 $k_{\text{B}}T$, which is shown in Fig. 3.

B. Kinetic fits to simulation

Fitting the simulation data validates the fitting software and underlying approach. Four simulations were run, with $\Delta c_{\text{PE}} = \{0, 0.14, 0.28, 0.34\}$ nm^{-1}, $\kappa = 33.78$ $k_{\text{B}}T$, and $D = 8$ μm^2/s. The bending modulus is overestimated slightly versus the input parameter (33.78–36.49 $k_{\text{B}}T$). The

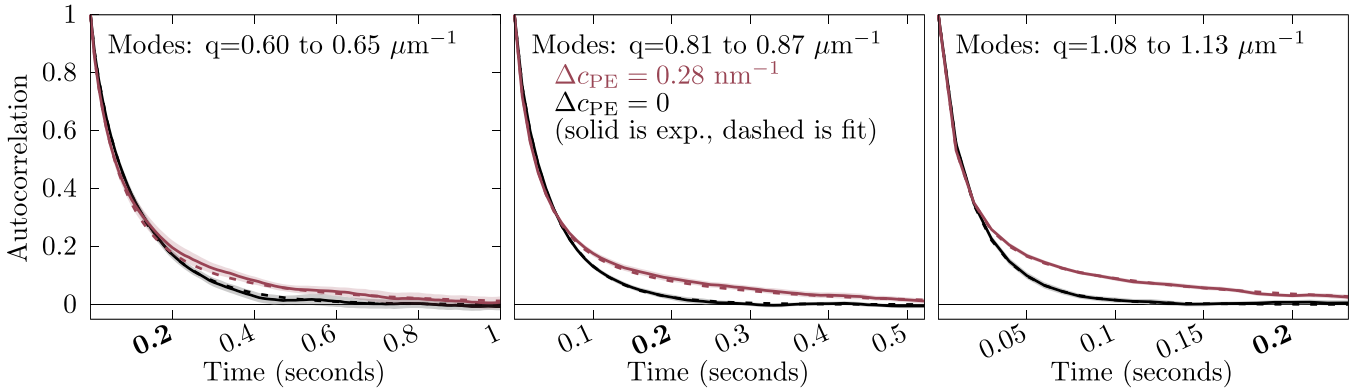

FIG. 4. The average of the autocorrelation $\langle v_q(t)v_q(0)\rangle$ over similar modes for the simulation (solid) and fits (dashed). POPC is colored in black. The $\Delta c_{PE} = 0.28$ nm^{-1} is colored red. The shaded regions indicate two standard errors from the simulation obtained by averaging over similar modes. The label at $t = 0.2$ s on all three plots is shown in bold for a common reference. Here $\kappa = 33.8 k_B T$ and $D = 8\,\mu$m^2/s.

diffusion constant is 8 μm^2/s within one standard error [Fig. 4]. Extracted spontaneous curvatures are slightly overestimated: $\{0.02, 0.16, 0.30, 0.36\} \pm 0.003$ nm^{-1}, in each case 0.02 nm^{-1} too high.

The autocorrelation function for each in-plane projected mode is fit to its model kinetics [Eq. (41)]. Averaging multiple autocorrelation functions together (for modes with similar dynamics) illustrates the separate undulation and diffusion time scales better than noisy individual fits. Average autocorrelation functions for three q ranges are shown in Fig. 4, as well as the averages for the fits. The fit curves shown are solved for the $\Delta c_{PE} = 0.28$ nm^{-1} data set, adjusting single values of κ, D, and c_0 applicable to all fit curves for a data set. For the simulation, fast noise is set to zero as this term only models experimental noise. Error bars are computed by statistical analysis of the correlation functions, assuming the same kinetics.

The difference between the red (light gray) and black curves at long time illustrates the effect of curvature-coupled lipid diffusion on the undulation relaxation timescale. The agreement of the fits and input model parameters indicates that the fitting procedure is robust for simulation data with the same information content as the experiment.

C. Kinetic fits to GUV microscopy

Average autocorrelation functions for the same three q-ranges above are now shown in Fig. 5 for the undulations recorded by GUV microscopy, as well as the averages for the fits. While like the simulations the single fit shares mechanical parameters between autocorrelation functions, now each autocorrelation function has its own parametrization of the fast noise. Before plotting, the fast noise was subtracted from the autocorrelation function, the average was computed, and, finally, renormalized.

Fitting the mechanical parameters of the PE-PC mixture yields $\kappa = 29.90 \pm 1.01\ k_B T$, $D = 8.2 \pm 0.4\,\mu$m^2/s, and $\Delta c_{PE} = 0.340 \pm 0.01$ nm^{-1}. For the fit to POPC, $\kappa = 26.35 \pm 0.85\, k_B T$, $D = 1.1 \pm 0.2\,\mu$m^2/s, and $\Delta c_{PE} = 0.16 \pm 0.007$ nm^{-1}. Note that for the pure POPC GUVs, D and Δc_{PE} should not be part of the mechanism, and therefore, Δc_{PE} should be zero with D unresolvable. We believe that, for POPC, these values are indicative of overfitting, that is, the use of nonsensical parameters that fit stochastic error in the experiment and systematic error in the model. The fits indicate that, in contrast to $\kappa_{apparent}$, κ is similar for the PE-PC and POPC samples. Furthermore, the difference in Δc_{PE} for the two samples compares well to the expected spontaneous curvature of DOPE (-0.34 nm^{-1} [30]) and POPC (-0.02 nm^{-1} [31]).

If the whole range of available GUVs were selected for analysis, the average κ for POPC would be $32.095 \pm 1.18\ k_B T$ and $30.07 \pm 1.52\ k_B T$ for PE-PC. Spontaneous curvatures were similar to the reduced set (0.18 ± 0.01 nm^{-1} and 0.30 ± 0.007 nm^{-1} for POPC and PE-PC, respectively).

The fit results converge for the experiment when $t_{max,q}$ is sufficiently large (above 30 times τ_p), and for q_{max} greater than 1 μm^{-1}. Sensitivity of c_0 to $t_{max,q}$ and q_{max} are shown in Figs. S3 and S2 of the Supplemental Material [32].

The fit to the pure POPC shows slow time-scale relaxations; yet these are inconsistent with diffusional softening. Foremost, the apparent diffusion constant extracted (1.1 μm^2/s) is inconsistent with lipid diffusion, which is consistently measured to be much larger (approximately 8 μm^2/s and modestly reduced with cholesterol in disordered phases [33–36]). That is, the time scale is unlikely to be due to a contaminant or oxidated lipid. The time scale appears too small to be a result of lipid flip flop, whose characteristic time scale is on the order of hours [37]. Although the mechanism for the small amplitude slow relaxation in pure POPC is unknown, the effect is larger in PE-PC. While Δc_{PE} for PE-PC and POPC (0.340 nm^{-1} and 0.16 nm^{-1}) appear comparable, the strength of the effect goes as Δc_{PE}^2, and thus is over four times larger for PE-PC.

D. Implication of diffusional softening

Fitting the distribution of undulation magnitudes is sensitive to $\kappa_{apparent}$. Fitting undulation kinetics extracts κ, D, and Δc_{PE}^2. As presented here, κ only accounts for diffusional softening; structural dynamics that couple to curvature at faster time scales affect κ.

Kinetic fitting of GUVs demonstrates that the PE-PC mixture has κ, D, and Δc_{PE} consistent with previous

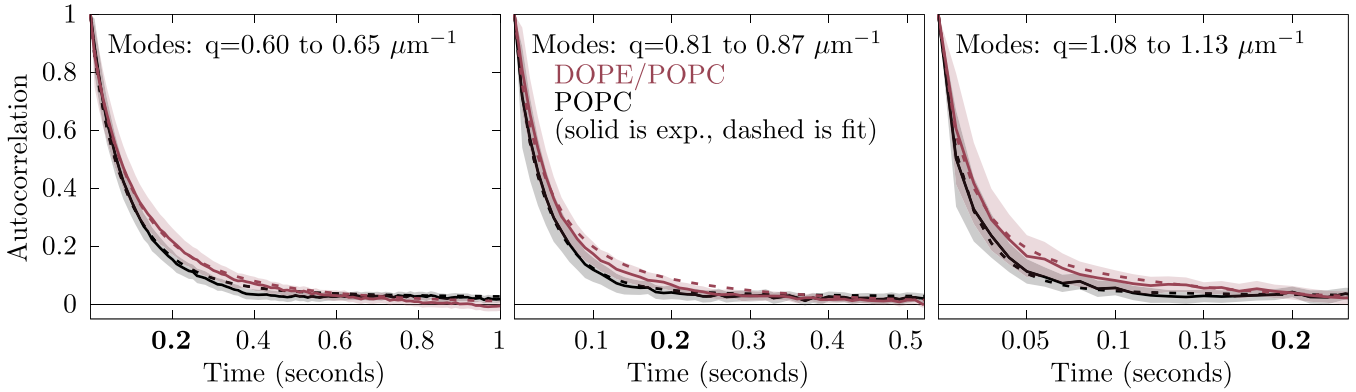

FIG. 5. The average of the autocorrelation $\langle v_q(t)v_q(0)\rangle$ over similar modes for the experiment (solid) and fits (dashed). POPC is colored in black. The DOPE-POPC mixture is colored red. Filled curves indicate two standard errors from the experiment obtained by averaging over similar modes.

measurements of spontaneous curvature [30] and diffusion [34], as well as a minimal difference, if any, for κ relative to POPC. That is, the larger and somewhat slower undulations of the PE-PC mixture are consistent not with a change in the underlying softness of the bilayer, but rather through the coupling of the spontaneous curvature of DOPE to dynamic undulations.

Separating mechanistic contributions to κ_{apparent} is critical for developing a complete model of the membrane, including its equilibrium and nonequilibrium relaxation behavior. In the absence of the model of diffusional softening, extrapolating κ_{apparent} to 100% DOPE yields, relative to pure POPC, an extremely small value for pure DOPE, approximately 10.64 k_BT. In contrast, in the diffusional softening model, κ depends weakly on DOPE fraction. Note that while pure DOPE does not readily form lamellar phases at this temperature, its bending modulus in the hexagonal phase is 22–26k_BT, depending on the incorporation of interstitial tetradecane [30].

The principal indication of diffusional softening is the long-time-scale autocorrelation of the undulation amplitude. The initial fast undulation kinetics cannot be used reliably to determine κ; the undulation rate k_+ is reduced by coupling to diffusion (by $\alpha\tau_p^{-1}$). The impact of this friction is reduced at high q as τ_p grows relative to τ_m.

E. GUV relaxation kinetics as a probe for structural heterogeneity

Any structure with curvature coupling different from the bulk will influence the magnitude and kinetics of GUV fluctuations. Thus, in theory, kinetics can be used to infer the dynamics and coupling strength of complex structures such as nanodomains and lipid multimers. Coupling of GM1 to curvature is a plausible explanation for the dramatic softening of POPC-GM1 mixtures [38], where at mol fractions less than 10% GM1 the bending modulus is less than 25% of that of pure POPC. Such softening could indicate that size (A_p) and/or coupling strength (Δc_{PE}) of the GM1-enriched structural unit exceeds that of a typical lipid. The proximity of the gel-fluid transition suggests the possibility of curvature-sensitive GM1 multimers.

Experiments clearly indicate liquid ordered domains have increased κ compared with disordered phases [7]. The magnitude of the effect is likely sufficiently large that the linearized treatment of the coupling α is inadequate. For stiff domains that couple strongly to curvature, α quickly becomes larger than one, indicating a breakdown in the theory. Indeed softening is nonlinear above 5 mol% GM1 in POPC.

IV. CONCLUSION

The dynamic coupling of the lateral distribution of curvature-sensitive lipids to membrane undulations leads to diffusional softening of the membrane [12,15,18,21]. The undulation autocorrelation function implies the intrinsic bending rigidity of the membrane, the diffusion constant of the underlying lipids, and the magnitude of the spontaneous curvature difference (through the time scale). The intrinsic bending rigidity of the membrane determined from the kinetics is related to the apparent bending rigidity determined from the fluctuation spectrum through the softening factor. The experiment and model corroborate a similar experiment on membrane nanotubes by Bashkirov *et al.* [21], in which DOPE also softened a majority PC bilayer according to Eq. (25).

A key factor of the diffusional softening mechanism is how coupling of undulations to diffusion acts as a friction. The impact of this force depends on q. The response of membrane undulations to this frictional force is observed in the relaxation kinetics of membrane undulations. Membrane viscosity [39] and interleaflet friction [40,41] also influence membrane undulation kinetics at shorter time scales. Understanding how undulation kinetics is modified by these terms has proved crucial for understanding the fine mechanisms of membrane shape dynamics [42].

It is critical to understand the extent of this mechanism when inferring the bending modulus of complex mixtures. For example, conflicting results have recently been published for the bending modulus of cholesterol in DOPC. Neutron spin-echo experiments, which probe relaxation times of bilayers below the time scale of diffusion, indicate the bilayer is stiffer [43]. Yet multiple techniques that probe equilibrium fluctuations have shown that κ_{apparent} is unchanged [8,19,29,44]. Hexagonal phase experiments indicate

that cholesterol will have a high negative spontaneous curvature in fluid bilayers [30]. Accepting the diffusional softening mechanism, cholesterol is expected to soften a DOPC bilayer, in the absence of a stiffening effect. Note however, that to fully resolve the reported discrepancy, membrane viscosity contributions in time-correlation analysis should be interrogated; recent analysis indicates that viscosity affects a broader array of undulations of smaller liposomes than previously anticipated, suggesting another possible change in the interpretation of spin-echo experiments [39].

GUV fluctuations suggest that cholesterol at 10 mol% reduces the κ_{apparent} of SOPC, while increasing κ_{apparent} at higher concentrations [45]. X-ray derived data contradicts this [44]. In either case the effect is sufficiently small as to be difficult to statistically distinguish. Hexagonal phase experiments with variable osmotic stress (a technique for which lateral redistribution is irrelevant) indicate cholesterol stiffens DOPC and DOPE somewhat. Considering diffusional softening, it is possible that cholesterol is both stiffening the underlying κ while lowering κ_{apparent} such that the change is minimal. Interpreting neutron spin-echo experiments [46] is challenging [47]. Indeed other interpretations of the discrepancy between equilibrium and kinetic techniques are plausible, such as cholesterol-driven changes in the neutral surface of bending or the area compressibility independent of the bending modulus [48]. This case illustrates the importance of deducing the molecular mechanism of changes in bilayer stiffness.

Data files of the GUV fluctuations, along with the software to simulate and fit their kinetics, are publicly available [49].

ACKNOWLEDGMENTS

K.S. and A.J.S. were supported by the intramural research program of the Eunice Kennedy Shriver National Institutes of Child Health and Human Development (NICHD) at the National Institutes of Health. M.A. acknowledges funding from International Max Planck Research School on Multiscale Bio-Systems (IMPRS). This research was also supported in part by the National Science Foundation under Grant No. NSF 600 PHY-1748958.

[1] R. Dimova and C. M. Marques (Eds.), *The Giant Vesicle Book* (CRC Press, Boca Raton, 2019)
[2] W. Helfrich, Z. Naturforschung - Section C: J. Biosc. **28**, 693 (1973).
[3] P. B. Canham, J. Theor. Biol. **26**, 61 (1970).
[4] H. A. Faizi, C. J. Reeves, V. N. Georgiev, P. M. Vlahovska, and R. Dimova, Soft Matter **16**, 8996 (2020).
[5] E. A. Evans, Biophys. J. **43**, 27 (1983).
[6] E. Evans and W. Rawicz, Phys. Rev. Lett. **64**, 2094 (1990).
[7] T. Baumgart, S. Das, W. W. Webb, and J. T. Jenkins, Biophys. J. **89**, 1067 (2005).
[8] B. Sorre, A. Callan-Jones, J. B. Manneville, P. Nassoy, J. F. Joanny, J. Prost, B. Goud, and P. Bassereau, Proc. Nat. Acad. Sci. USA **106**, 5622 (2009).
[9] R. Dasgupta, M. S. Miettinen, N. Fricke, R. Lipowsky, and R. Dimova, Proc. Natl. Acad. Sci. USA **115**, 5756 (2018).
[10] R. Lipowsky, Faraday Discuss. **161**, 305 (2013).
[11] H. J. Lessen, K. C. Sapp, A. H. Beaven, R. Ashkar, and A. J. Sodt, Biophys. J. **121**, 3188 (2022).
[12] I. Bivas and P. Méléard, Phys. Rev. E **67**, 012901 (2003).
[13] V. Vitkova and C. Misbah, Adv. Planar Lipid Bilayers Lipo. **14**, 257 (2011).
[14] E. Reister-Gottfried, S. M. Leitenberger, and U. Seifert, Phys. Rev. E **81**, 031903 (2010).
[15] S. Leibler, J. Phys. **47**, 507 (1986).
[16] V. Vitkova, J. Genova, M. D. Mitov, and I. Bivas, Mol. Cryst. Liq. Cryst. **449**, 95 (2006).
[17] S. Tristram-Nagle and J. F. Nagle, Biophys. J. **93**, 2048 (2007).
[18] M. M. Kozlov and W. Helfrich, Langmuir **8**, 2792 (1992).
[19] A. Tian, B. R. Capraro, C. Esposito, and T. Baumgart, Biophys. J. **97**, 1636 (2009).
[20] P. V. Bashkirov, P. I. Kuzmin, J. Vera Lillo, and V. A. Frolov, Ann. Rev. Biophys. **51**, 473 (2022).
[21] P. V. Bashkirov, K. V. Chekashkina, S. A. Akimov, P. I. Kuzmin, and V. A. Frolov, Biochem. (Moscow) A **5**, 205 (2011).
[22] A. Imparato, J. C. Shillcock, and R. Lipowsky, Europhys. Lett. **69**, 650 (2005).
[23] G. Brannigan and F. L. Brown, J. Chem. Phys. **122**, 074905 (2005).
[24] R. Dimova, B. Pouligny, and C. Dietrich, Biophys. J. **79**, 340 (2000).
[25] R. Dimova, Adv. Colloid Interface Sci. **208**, 225 (2014).
[26] K. C. Sapp, A. H. Beaven, and A. J. Sodt, Phys. Rev. E **103**, 042413 (2021).
[27] M. I. Angelova and D. S. Dimitrov, Faraday Discuss. Chem. Soc. **81**, 303 (1986).
[28] R. Dimova, Ann. Rev. Biophys. **48**, 93 (2019).
[29] R. S. Gracià, N. Bezlyepkina, R. L. Knorr, R. Lipowsky, and R. Dimova, Soft Matter **6**, 1472 (2010).
[30] Z. Chen and R. P. Rand, Biophys. J. **73**, 267 (1997).
[31] B. Kollmitzer, P. Heftberger, M. Rappolt, and G. Pabst, Soft Matter **9**, 10877 (2013).
[32] See Supplemental Material at http://link.aps.org/supplemental/10.1103/PhysRevE.107.054403 for a movie of a GUV fluctuation, dependence of the fit on the maximum q and time, as well as comparison of a broad range of experimental undulation autocorrelation functions.
[33] P. F. Fahey, D. E. Koppel, L. S. Barak, D. E. Wolf, E. L. Elson, and W. W. Webb, Science **195**, 305 (1977).
[34] H. C. Gaede and K. Gawrisch, Biophys. J. **85**, 1734 (2003).
[35] H. A. Scheldt, D. Huster, and K. Gawrisch, Biophys. J. **89**, 2504 (2005).
[36] F. Heinemann, V. Betaneli, F. A. Thomas, and P. Schwille, Langmuir **28**, 13395 (2012).
[37] D. Marquardt, F. A. Heberle, T. Miti, B. Eicher, E. London, J. Katsaras, and G. Pabst, Langmuir **33**, 3731 (2017).
[38] N. Fricke and R. Dimova, Biophys. J. **111**, 1935 (2016).

[39] H. A. Faizi, R. Dimova, and P. M. Vlahovska, Biophys. J. **121**, 910 (2022).
[40] R. L. Schoch, I. Barel, F. L. Brown, and G. Haran, J. Chem. Phys. **148**, 123333 (2018).
[41] A. Zgorski, R. W. Pastor, and E. Lyman, J. Chem. Theory Comput. **15**, 6471 (2019).
[42] M. Nagao, E. G. Kelley, R. Ashkar, R. Bradbury, and P. D. Butler, J. Phys. Chem. Lett. **8**, 4679 (2017).
[43] S. Chakraborty, M. Doktorova, T. R. Molugu, F. A. Heberle, H. L. Scott, B. Dzikovski, M. Nagao, L. R. Stingaciu, R. F. Standaert, F. N. Barrera, J. Katsaras, G. Khelashvili, M. F. Brown, and R. Ashkar, Proc. Nat. Acad. Sci. USA **117**, 21896 (2020).
[44] J. Pan, S. Tristram-Nagle, and J. F. Nagle, Phys. Rev. E **80**, 021931 (2009).
[45] J. Genova, V. Kralj-Iglič, A. Iglič, R. Marinov, and I. Bivas, J. Phys.: Conf. Ser. **398**, 012037 (2012).
[46] A. G. Zilman and R. Granek, Chem. Phys. **284**, 195 (2002).
[47] M. C. Watson and F. L. Brown, Biophys. J. **98**, L9 (2010).
[48] J. F. Nagle, Phys. Rev. E **104**, 044405(2021).
[49] A. Sodt and K. Sapp, OSF (2023), doi: 10.17605/OSF.IO/XHN69.